JACS
JOURNAL OF THE AMERICAN CHEMICAL SOCIETY
Article
pubs.acs.org/JACS

Reactions of Persistent Carbenes with Hydrogen-Terminated Silicon Surfaces

Aleksandr V. Zhukhovitskiy,[†] Michael G. Mavros,[†] K. T. Queeney,[§] Tony Wu,[†,‡] Troy Van Voorhis,[†] and Jeremiah A. Johnson*[,†]

[†]Department of Chemistry, and [‡]Department of Electrical Engineering and Computer Science, Massachusetts Institute of Technology, Cambridge, Massachusetts 02139, United States

[§]Department of Chemistry, Smith College, Northampton, Massachusetts 01063, United States

Supporting Information

ABSTRACT: Surface passivation has enabled the development of silicon-based solar cells and microelectronics. However, a number of emerging applications require a paradigm shift from passivation to functionalization, wherein surface functionality is installed proximal to the silicon surface. To address this need, we report here the use of persistent aminocarbenes to functionalize hydrogen-terminated silicon surfaces via Si−H insertion reactions. Through the use of model compounds (H−Si(TMS)$_3$ and H−Si(OTMS)$_3$), nanoparticles (H−**SiNPs**), and planar Si(111) wafers (H−**Si(111)**), we demonstrate that among different classes of persistent carbenes, the more electrophilic and nucleophilic ones, in particular, a cyclic (alkyl)(amino)carbene (CAAC) and an acyclic diaminocarbene (ADAC), are able to undergo insertion into Si−H bonds at the silicon surface, forming persistent C−Si linkages and simultaneously installing amine or aminal functionality in proximity to the surface. The CAAC (**6**) is particularly notable for its clean insertion reactivity under mild conditions that produces monolayers with 21 ± 3% coverage of Si(111) atop sites, commensurate with the expected maximum of ∼20%. Atomic force and transmission electron microscopy, nuclear magnetic resonance, X-ray photoelectron, and infrared spectroscopy, and time-of-flight secondary ion mass spectrometry provided evidence for the surface Si−H insertion process. Furthermore, computational studies shed light on the reaction energetics and indicated that CAAC **6** should be particularly effective at binding to silicon dihydride, trihydride, and coupled monohyride motifs, as well as oxidized surface sites. Our results pave the way for the further development of persistent carbenes as universal ligands for silicon and potentially other nonmetallic substrates.

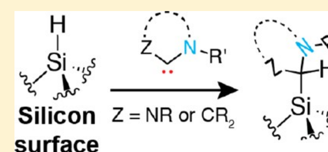

I. INTRODUCTION

The properties of materials are often dictated in large part by their surface functionality.[1−5] Currently, the methods available for controlled surface modification are not as well developed as solution synthetic methodologies. Furthermore, surface functionalization methods are generally limited in their substrate scope: surface anchors that bind strongly to metals are rarely suitable for nonmetals or metal oxides and vice versa. Given these limitations, there is continued need for surface anchors that are more universal in scope and that facilitate precise control over surface functionality.

One of the most demanding surfaces in this regard is that of silicon, on which the present-day semiconductor industry is largely founded. Silicon surfaces, and in particular, their defects, play an active role in charge recombination, a generally undesirable process that leads to reduced device performance.[6] Although this challenge has been partially addressed through organic and/or inorganic surface passivation routes (i.e., via formation of Si−C bonds[7−13] or Si−H/heteroatom bonds,[14,15] respectively), the continued evolution of silicon-based technologies will require new methods for the precise and controlled introduction of surface functionality.

Although traditional silicon passivation routes have enabled the incorporation of useful functional groups into surface-grafted monolayers, these functional groups are generally separated from the surface via long insulating alkane spacers.[16,17] In many applications, a preferred design would utilize a short, perhaps one-carbon, spacer between the surface and the functionality; it would provide a thermally and hydrolytically stable surface anchor while at the same time permitting through-bond/-space electronic coupling between the functional group and the surface.

Recent reports demonstrated that amines are highly versatile functional groups for modulating the properties of surfaces, including silicon.[18,19] However, covalent attachment of amines to silicon via a one-carbon spacer is presently not feasible using conventional hydrosilylation[12,13] of imines, and no reports exist of nucleophilic alkylation of silicon surfaces with thermally unstable *N*,*N*-disubstituted aminomethyllithium reagents.[20] Application of retrosynthetic analysis to this surface-modification challenge revealed a simple disconnection (Figure 1), which in the forward sense amounts to amino-carbene insertion into the Si−H bonds of a H-terminated silicon surface (H−**Si**). Notably, both the proposed carbene and the surface are readily accessible reagents; the use of such carbenes as surface anchors in other contexts has been recently reviewed.[21,22]

Received: May 13, 2016
Published: July 1, 2016

 © 2016 American Chemical Society

DOI: 10.1021/jacs.6b04962
J. Am. Chem. Soc. 2016, 138, 8639−8652

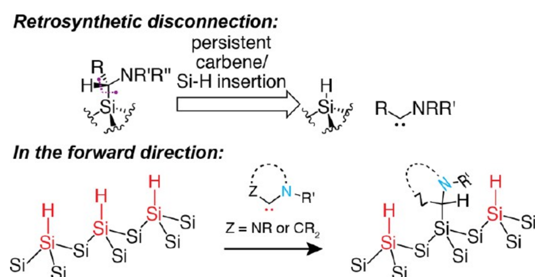

Figure 1. Concept.

Carbene insertion presents an intriguing mechanistic approach to H−**Si** functionalization. To our knowledge, the only two existing examples involve highly reactive, non-persistent carbenes. First, Tilley and co-workers reported on the treatment of H−**Si(111)** (H-terminated silicon (111)) with dichlorocarbene.[23] Although very promising, this method could be limited by the use and generation of Hg-containing species, as well as the concomitant uncontrolled chlorination and bromination of the silicon surface.[23] Second, Ghadiri and co-workers reported on Rh-catalyzed carbenoid insertion on H-terminated porous silicon surfaces.[24] This approach enables the use of a wide-range of carbene precursors (diazo compounds), but hinges on the use of transition metal catalysis, which may or may not be feasible in certain applications.[24] Furthermore, lack of precedence for α-amino-α-diazo compounds or α-amino-methylmercury reagents renders the above methods incapable of installing amines with one-carbon spacers. Although another study purported to use persistent diaminocarbenes to stabilize Si nanoparticle (SiNP) surfaces,[25] to our knowledge the insertion reactivity of persistent carbenes in the context of H-terminated silicon surfaces has not been explored. As discussed above, persistent aminocarbene, for example, *N*-heterocyclic carbene (NHC), insertion would provide a natural entry into the desired amine-functionalized silicon surfaces (Figure 1).

Interest in the insertion reactivity of persistent carbenes has surged in the last 15 years; controlled bond insertion is a promising strategy to cleave H−H, C−H, and heteroatom−H bonds that are difficult to cleave by homo- and heterolysis. Particularly intriguing to us was the discovery by Bertrand and co-workers that persistent singlet NHCs readily undergo insertion into the Si−H bonds of phenylsilane, diphenylsilane, and triethoxysilane.[26] Soon after, Radius and co-workers described an insertion/ring-expansion cascade in NHC−silane systems,[27] and Bielawski and co-workers extended the silane insertion reactivity to diamidocarbenes (DACs).[28] Inspired by these reports, and given our vision of persistent carbenes as potentially universal surface anchors,[21,29,30] we set out to explore them in the context of H−**Si** modification.

II. MODEL COMPOUND STUDIES

The exploration of new reactions on surfaces can be critically informed by analogous homogeneous reactions with model compounds whose structures map well onto surface fragments. From such studies, one can gain valuable insights about relative reaction kinetics and thermodynamics, potential side reactions, and structural features of the product(s) that could extrapolate to surfaces; such information would be challenging to extract from direct surface studies. The model compound strategy also allows for a rapid screening of reactants and conditions to identify the optimal one(s) to be adapted to surfaces. For H−**Si** surfaces, we supposed that tris(trimethylsilyl)silane (TTMSS, Figure 2) would be an expedient model compound, because the electronic and steric environment of the Si−H bond in TTMSS

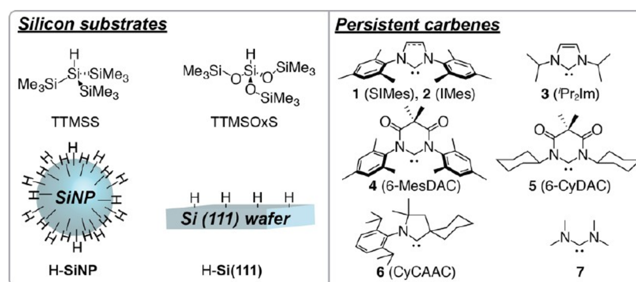

Figure 2. Silicon substrates and carbenes employed in this study.

closely approximates that of the H−**Si(111)** surface.[31] Additionally, TTMSS is an inexpensive, stable, and commercially available compound. Finally, the oxidized analogue of TTMSS, TTMSOxS (Figure 2), is expected to be a good model of backbond-oxidized silicon surface regions.

During initial screens, carbene **2** (IMes, 55 mM) was found to be unreactive toward TTMSS even after 48 h at 80 °C in benzene-d^6. Under the same conditions, carbene **1** (SIMes) underwent partial cycloelimination[32] with no evidence of insertion. We initially hypothesized that the steric bulk surrounding the Si−H bond in TTMSS inhibited the insertion of NHCs with bulky *N*-substituents. However, exposure of less sterically encumbered carbene **3** (^{i}Pr$_2$Im, 35 mM) to TTMSS in benzene-d^6 at 80 °C for 6 d afforded no insertion products within the limit of detection of ^{1}H nuclear magnetic resonance (NMR) spectroscopy. Although, in the context of silane insertion, the saturated analogue of **3** (^{i}Pr$_2$ImH$_2$) was expected to be more reactive than **3** on the grounds of analogous observations for DippH$_2$ (=SIPr) versus Dipp (=IPr),[26,27] the propensity of ^{i}Pr$_2$ImH$_2$ to dimerize led us to exclude it from this initial carbene screen.[33] (Note that specialized conditions have enabled the preparation of ^{i}Pr$_2$ImH$_2$ in a way that precludes rapid dimerization, and may enable the use of this carbene in future surface functionalization studies.[34]) In any event, although the steric bulk of the tested NHCs may have been prohibitive in this system, we hypothesized that the nucleo- and/or electrophilicity of these diamino-NHCs was also insufficient to enable Si−H insertion.

To address this hypothesis, we turned to more electrophilic (and somewhat less electron-donating,[35,36] albeit comparably basic[37]) diamidocarbenes (DACs).[35,36,38] Initial studies with *N*,*N*′-dimesityl DAC (**4**, MesDAC)[35] provided little evidence of carbene insertion into the Si−H bond of TTMSS: ^{1}H NMR spectroscopy indicated that no insertion took place at 23 °C, and even after 22 h at 80 °C, only ∼5% of TTMSS was converted to an unidentified new species with a higher frequency (more downfield) TMS methyl resonance. Meanwhile, the concomitant extensive (∼77%) decomposition of **4** via intramolecular benzylic C−H insertion[39] rendered further investigation of this compound imprudent.

Given that the large steric bulk of **4** was a potential obstacle for the Si−H insertion, we sought to prepare a DAC with reduced steric bulk surrounding the carbene. While to our knowledge all reported examples of DACs have large *N*-aryl substituents, we wondered if we could replace them with smaller *N*-alkyl ones; we were particularly inspired by reports of “flexible” steric bulk in the context of NHCs by Glorius and co-

DOI: 10.1021/jacs.6b04962
J. Am. Chem. Soc. 2016, 138, 8639−8652

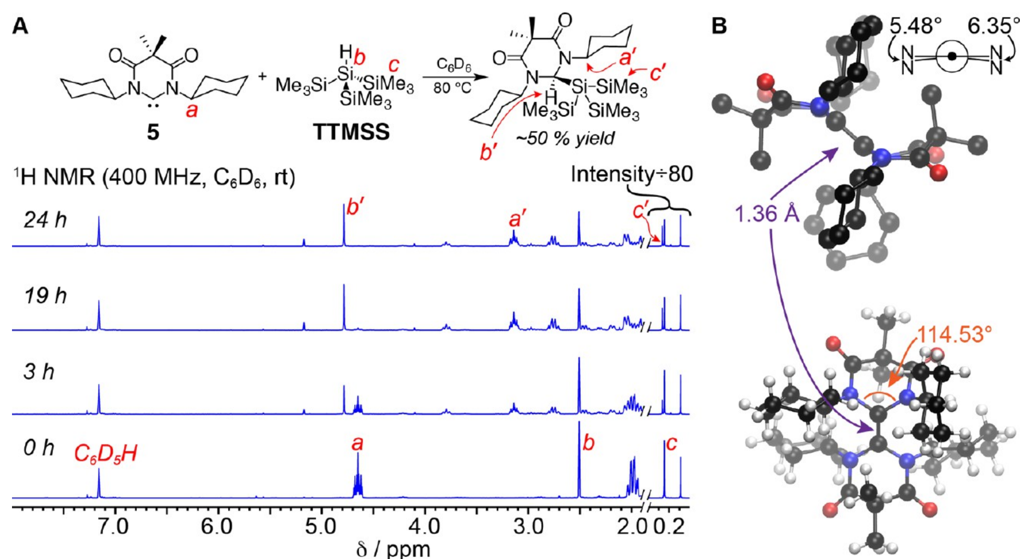

Figure 3. (A) Monitoring insertion of **5** into the Si–H bond of TTMSS by ^{1}H NMR. (B) X-ray crystal structure of the dimer of **5** ($(\mathbf{5})_2$), shown from two perspectives (hydrogen atoms not shown in the upper structure for clarity). Hydrogen atoms are in white, carbon in black, nitrogen in blue, and oxygen in red.

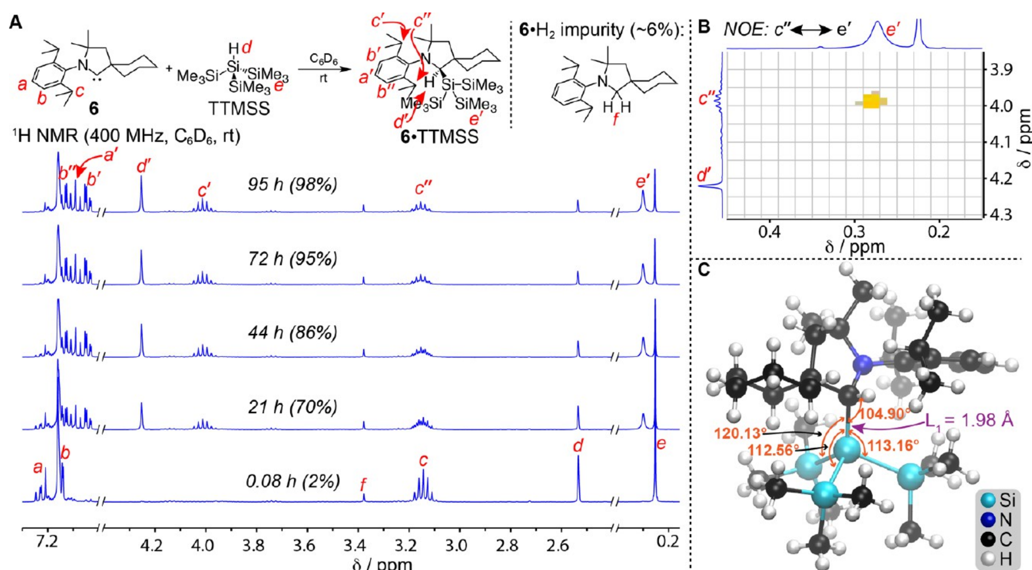

Figure 4. (A) ^{1}H NMR analysis of the insertion reaction between **6** and TTMSS. (B) Excerpt of the NOESY spectrum of the insertion product, showing an interaction between protons *c″* and *e′*. (C) X-ray crystal structure of **6**·TTMSS.

workers.[40,41] Specifically, given the conformational freedom of cyclohexyl groups, we anticipated that they might provide the ideal combination of sufficient steric bulk to inhibit DAC dimerization with the flexibility needed for DAC insertion into the Si–H bond of TTMSS. Intramolecular C–H insertion by the carbene was also expected to be minimal due to the absence of accessible activated C–H bonds.

N,*N*′-Dicyclohexyl DAC (**5**) was successfully prepared following conditions analogous to the method utilized by Hudnall and Bielawski[36] for the synthesis of *N*,*N*′-daryl DACs (e.g., **4**). NaHMDS was employed as the base to generate the free carbene. The latter displayed no sign of degradation in C_6D_6 solution at 0.16 M concentration during the course of at least 3 h at 23 °C, and exhibited a characteristic carbene carbon ^{13}C NMR resonance at 269.5 ppm (see the Supporting Information).

After exposure of a 0.164 M solution of **5** in C_6D_6 to TTMSS at 23 °C, no reaction was noted by ^{1}H NMR during the course of 3 h. However, elevation of the temperature to 80 °C led to simultaneous consumption of the carbene and TTMSS and the appearance of new resonances corresponding to the insertion product (Figure 3A). The transformation was complete in 24 h, and the identity of the insertion product was unequivocally established through Fourier transform ion cyclotron resonance mass spectrometry (FTICR-MS) and a combination of 2-D NMR techniques (gCOSY, HSQC, gHMBC, and NOESY), in addition to 1-D NMR characterization (see the Supporting Information). Attempts to crystallize this product failed. Although this first observation of extensive carbene insertion into the Si–H bond of TTMSS was exciting, the product was formed in only ~50% yield (by NMR), and the remainder of the carbene was consumed by side reactions. One such side reaction was identified as the formal insertion of **5** into the N–

DOI: 10.1021/jacs.6b04962
J. Am. Chem. Soc. 2016, 138, 8639–8652

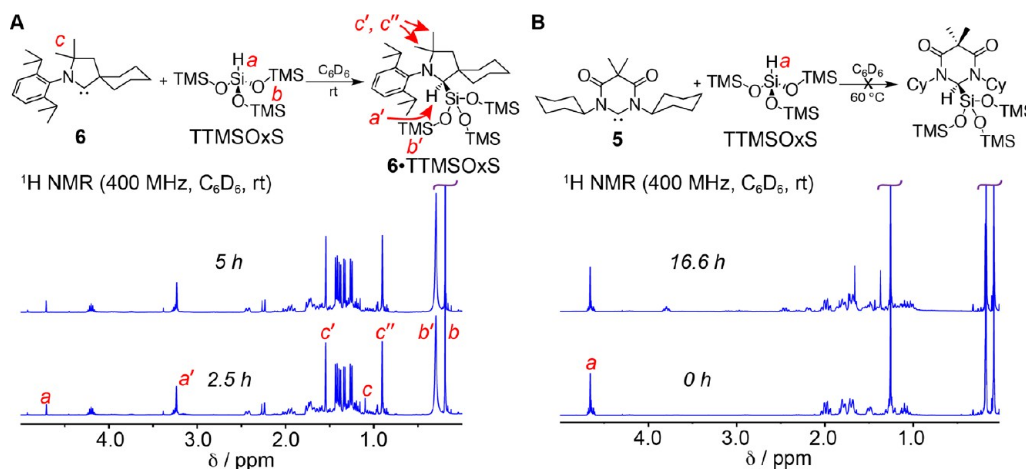

Figure 5. (A,B) Comparison of the insertion reactivity of **6** (A) and **5** (B) toward TTMSOxS, monitored by ^{1}H NMR spectroscopy.

H bond of HMDS (see the Supporting Information for details), which was generated during deprotonation of **5**·HOTf with NaHMDS. Examples of persistent carbene (including DAC) insertions into N−H bonds are well-known,[42−47] so our observation of this reactivity for **5** was not surprising. Another side reaction was the dimerization of **5** to yield a tetraamidoolefin, which was rather insoluble in C_6D_6 and readily crystallized (Figure 3B) or precipitated out of solution. The double bond character of the bond linking the two units of **5** in $(\mathbf{5})_2$ was apparent from its length of 1.36 Å[48] as well as the near coplanarity of the four nitrogen atoms attached to the olefin. Reduction of the reaction temperature to 60 °C did not alleviate the observed side processes. In particular, during preliminary H−**Si(111)** insertion experiments, we found that deposition of the poorly soluble dimer on silicon surfaces was a major complication, which compelled us to continue our search for better-suited persistent carbenes.

Although **5** was not ideally suited for H−**Si** surface functionalization via insertion, its reasonable success in the context of TTMSS insertion confirmed the benefit of elevated carbene electrophilicity in combination with steric flexibility. Informed by the insightful studies from Bertrand and co-workers[46] into H−H insertion by cyclic (alkyl)(amino)carbenes (CAACs)s and later Bielawski and Moerdyk[39] into intermolecular "non-acidic" C−H insertion by DACs, we speculated that insertion of carbenes into weakly polarized Si−H bonds would require that the carbene first nucleophilically polarize the Si−H and activate it for insertion. Thus, we wondered if persistent carbenes with both elevated electro- and nucleophilicity would more rapidly insert into the Si−H bond of TTMSS.

CAACs[49−54] are known to be more nucleophilic and more electrophilic than typical cyclic diaminocarbenes.[46,55] Among the known variants, **6**[54] was chosen for its flexible steric bulk. Exposure of **6** (0.046 M in C_6D_6, ∼85% purity by ^{1}H NMR) to 1.13 equiv of TTMSS at 23 °C resulted in 95% conversion (NMR yield = 95%) to the Si−H insertion product in 3 d as indicated by ^{1}H NMR spectroscopy (Figure 4A); during the first 44 h (86% conversion), the reaction followed second-order kinetics ($k_2^{23\,°C}$ = 2.0 M^{-1} h^{-1}, Figure S1). The structure of the product was first confirmed by a combination of 1-D and 2-D NMR spectroscopy and FTICR-MS (Figure 4A,B, and Supporting Information). An NOE interaction was observed for the trimethylsilyl protons *e*′ and the methine proton *c*″ (Figure 4B). The broadening of the TMS methyl resonance (Figure 4A) also suggested relatively slow, millisecond-time scale rotation of the tris(trimethylsilyl) group about the new Si−C bond. The identity of the product was verified by X-ray crystallography (Figure 4C) (crystals were grown in an NMR tube by slow DCM-d^2 evaporation in air at 23 °C.) The Si−$C_{carbene}$ bond length was 1.98 Å, the Si−$C_{carbene}$−H bond angle was 104.9°, and the three Si−Si−$C_{carbene}$ bond angles were 112.56°, 113.16°, and 120.13°; these structural parameters are analyzed further in section V.

The results from the model study with **6** confirmed our hypothesis that elevated carbene nucleo- and electrophilicity were critical for rapid TTMSS Si−H insertion. We also tested the insertion of **5** and **6** into the Si−H bond of TTMSOxS, and found that under reaction conditions identical to those used for TTMSS the insertion of **5** did not proceed, while that of **6** proceeded much more rapidly (Figures 5A,B); the reaction was essentially complete after 5 h. This difference in reactivity, which could stem from nucleophilic versus electrophilic polarization of the Si−H bond by these carbenes, could potentially allow for the development of site-selective functionalization of silicon surfaces.

Although **6** showed promise for Si−H insertion reactions on surfaces, we sought a carbene that could insert even more rapidly into the Si−H bond of TTMSS. Having surveyed the carbene literature, we recognized acyclic diaminocarbene (ADAC) **7**[34,56,57] as a promising candidate due to its reportedly increased nucleo- and electrophilicity as compared to **6**[55] and its considerably smaller steric bulk. Although as a free carbene, **7** decomposes with a half-life of a few hours at 0 °C in THF, it can be considerably stabilized toward decomposition by coordination to Li(I) species.[34,56,57] For instance, Alder and co-workers found that the use of a noncoordinating solvent (e.g., toluene-d^8) and a lithium base (e.g., lithium diisopropylamide (LDA) or lithium 2,2,6,6,-tetramethylpiperidine) or the addition of exogenous LiOTf could extend the half-life of **7** to many days at room temperature.[56] Guided by these precedents, we generated **7** by treatment of a suspension of **7**·HCl in toluene-d^8 at −78 °C with precooled solution of LDA in toluene-d^8 (concentration of **7**·HCl in toluene-d^8 is 0.15 M).

The insolubility of **7**·HCl resulted in relatively long reaction times (>10 min) even upon warming to 23 °C, which led to the simultaneous generation of **7**, its dimer $((\mathbf{7})_2)$,[34] and small quantities of unidentified side-products, as detected by ^{1}H NMR. Depending on whether more or less LDA was used, **7**

DOI: 10.1021/jacs.6b04962
J. Am. Chem. Soc. 2016, 138, 8639−8652

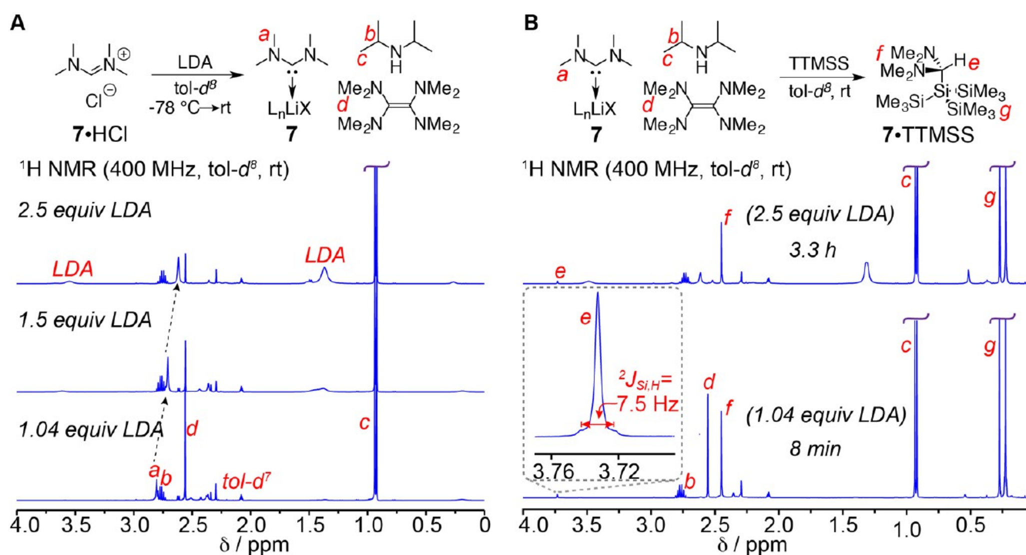

Figure 6. (A) Effect of LDA equivalents on the formation of **7** from **7**·HCl, judged by ^{1}H NMR spectroscopy. (B) ^{1}H NMR analysis of the reaction of **7** (generated using 1.04 or 2.5 equiv of LDA) with TTMSS to form **7**·TTMSS. Inset zooms in on the aminal methine proton *e* of **7**·TTMSS.

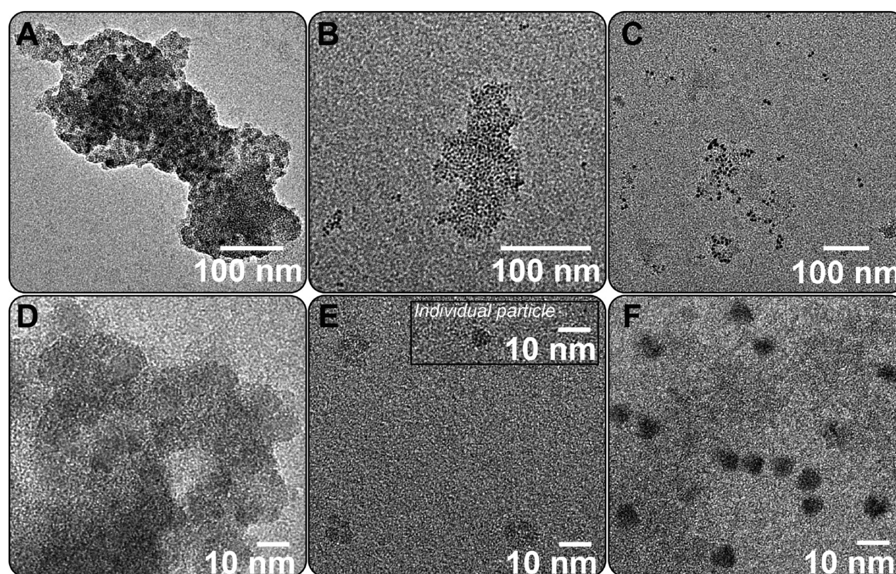

Figure 7. (A–F) TEM micrographs of H–**SiNPs** (A,D: zoomed in), **6**·**SiNPs** (B,E: zoomed in), and **7**·**SiNPs** (C,F: zoomed in). Inset in (E) illustrates an example of isolated **6**·**SiNPs** found on the TEM grid.

was accompanied by less or more dimer, respectively. To illustrate this behavior, when only 1.04 equiv of LDA was used, deprotonation was complete after 100 min, and the ratio **7**:(**7**)$_2$ was 2:1; **7** and (**7**)$_2$ combined constituted 50% of the **7**·HCl conversion (Figure 6A). In contrast, when 2.5 equiv of LDA was used, ~40 min was sufficient to complete the deprotonation, and the ratio of **7**:(**7**)$_2$ was 8.9:1 (Figure 6A). The ^{1}H NMR resonance corresponding to **7** shifted upfield from 2.80 to 2.62 ppm in the presence of excess LDA, confirming a substantial impact of **7**·Li^+ coordination in the latter case. Addition of 1 equiv of TTMSS (relative to **7**·HCl) to each of the solutions of **7** led to the consumption of the carbene via Si–H insertion (rapid relative to carbene dimerization), but at noticeably different rates: within 8 min, the reaction was already complete when 1.04 equiv of LDA was used, but when 2.5 equiv of LDA was used, 17.2 h was necessary to reach 89% conversion (Figure 6B). The insertion product has a methine proton with a characteristic singlet resonance at 3.73 ppm with satellite peaks arising due to the ^{29}Si–^{1}H coupling with $^2J_{Si,H}$ = 7.5 Hz, and its structure was verified by 1-D and 2-D NMR and FTICR-MS (Figure 6B, Supporting Information).

In the context of Si-surface functionalization (*vide infra*), we elected to use the conditions under which **7** was more reactive (1.04 equiv of LDA) because we sought rapid surface functionalization. As noted above, dimerization also proceeds under these conditions, but 26.5% of **7** remained after 4.5 h at 23 °C, so this background process was not expected to impact H–**Si** functionalization.

III. SiNP STUDIES

We next proceeded to explore carbene Si–H insertion in the context of SiNPs. H–**SiNPs** were prepared via the well-established sol–gel/hydrofluoric acid-etch method[58−61] (see the Supporting Information). H–**SiNPs** are known to be

DOI: 10.1021/jacs.6b04962
J. Am. Chem. Soc. 2016, 138, 8639−8652

difficult to disperse in organic solvents,[62] and, accordingly, only aggregates of particles could be observed by transmission electron microscopy (TEM) (Figure 7A). Attenuated total reflectance (ATR)-FTIR spectroscopy indicated that the produced H−**SiNPs** contained a mixture of surface silicon mono-, di-, and trihydride functional groups characterized by Si−H stretching resonances at 2081, 2098, and 2132 cm^{-1}, respectively (Figure 8A).[6,63] Additionally, ATR-FTIR detected

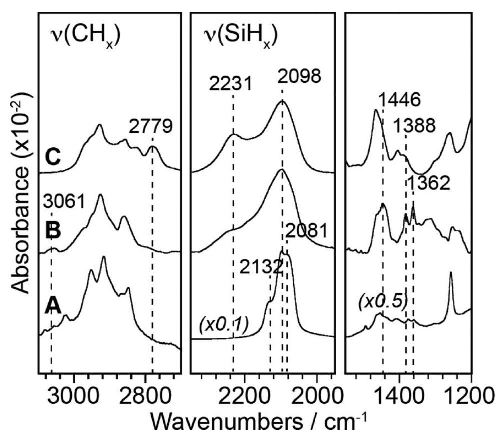

Figure 8. (A−C) ATR-FTIR spectra of H−**SiNPs** (A), **6·SiNPs** (B), and **7·SiNPs** (C). All absorbance values are relative to air.

a small Si−O stretch resonance centered at 1070 cm^{-1} (see the Supporting Information), consistent with the X-ray photoelectron spectroscopy (XPS) results (*vide infra*).

H−**SiNPs** were treated with **6** or **7** under reaction conditions similar to those of the model silanes (see the Supporting Information); in both cases, a reaction was evident from the gradual color change of the liquid phase from light yellow to dark brown. The two sets of isolated NPs (**6·SiNP** and **7·SiNPs**; see the Supporting Information) possessed notable differences in color and dispersibility: **6·SiNPs** changed from tan to dark brown upon drying *in vacuo*, while the **7·SiNPs** remained tan; furthermore, the latter were hardly redispersible in toluene-d^8, while the former were essentially completely redispersible in C_6D_6; the colloidal dispersion was stable on the time scale of hours, although precipitation was observed after ~2 d.

TEM of the dispersible fractions of both sets of NPs revealed more subtle differences between them (Figure 7B,C, and E,F): perhaps due to a thicker organic coating, **6·SiNPs** displayed lower contrast with the carbon film background as compared to **7·SiNPs** (Figure 7E,F); furthermore, while **7·SiNPs** were generally either isolated or paired (Figure 7C,F), **6·SiNPs** were observed isolated (Figure 7E, inset), in clusters of 3−4 overlapping NPs (Figure 7E), and in arrays of tens−hundreds of NPs (Figure 7B). Last, although both sets of NPs displayed a mixture of circular and triangular shapes, the two sets of particles exhibited differences in diameter distributions: 2.7 ± 0.5 nm for **6·SiNPs** versus 6.4 ± 1.7 nm for **7·SiNP** (each determined from measurement of 250 particles; Figures S2,S3). Similar NP size-selection due to the carbene steric bulk/curvature has been observed in previous studies of NHC-modified metal nanoparticles.[64,65]

ATR-FTIR (Figure 8) provided further evidence for the reactions of **6** and **7** with H−**SiNPs**. The relative intensities and frequencies of the specific CH_x stretching peaks in **6·SiNP** and **7·SiNP** are consistent with the attachment of **6** and **7** to SiNP surface sites. Two particularly notable differences in the CH_x regions between **6·SiNPs** and **7·SiNP** are (1) the resonance at ~3061 cm^{-1} present only in the spectrum of the former and (2) the resonance at ~2779 cm^{-1} present only in the spectrum of the latter. These have been assigned to the aromatic and aminal C−H stretches, respectively (*vide infra*). Additionally, carbene-specific spectral differences could also be observed in the region between 1550 and 1200 cm^{-1} (Figure 8): a pair of sharp resonances at 1362 and 1388 cm^{-1} and a broader resonance centered at 1446 cm^{-1} were present only in the spectrum of **6·SiNPs**; similar features shifted to higher

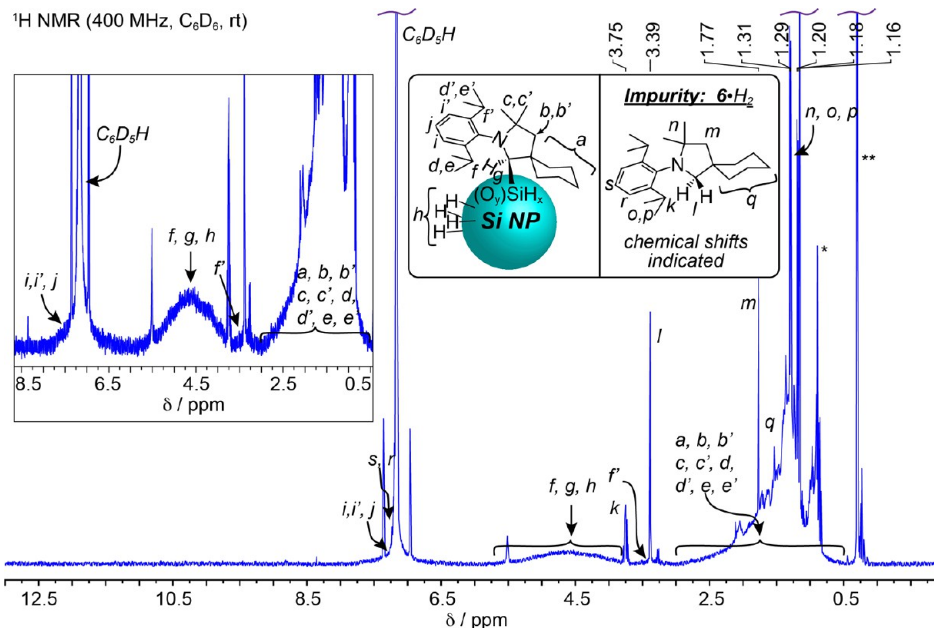

Figure 9. Solution ^1H NMR (400 MHz, C_6D_6, rt) spectrum of the redispersed **6**·SiNPs. Chemical shifts are indicated for the visible peaks corresponding to the trace **6**·H_2. Inset on the left zooms in on the broad resonances of **6**·SiNPs. *Hexanes resonances. **Silicone grease resonance.

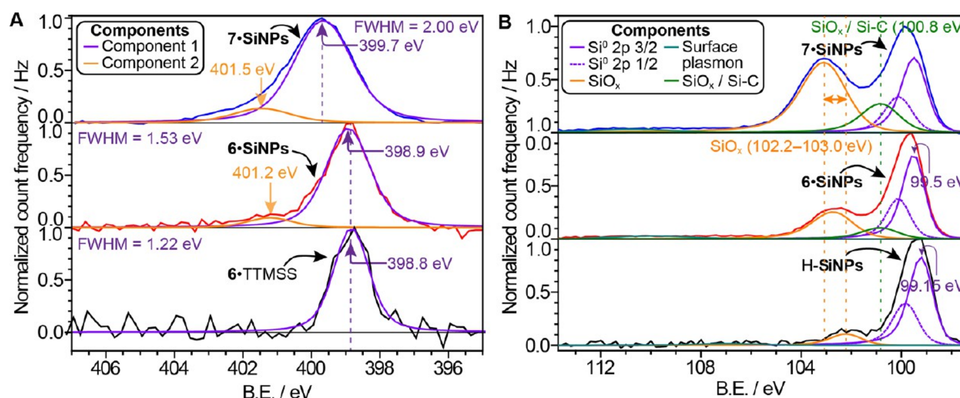

Figure 10. (A) Comparison of the XPS N 1s regions of **6·TTMSS**, **6·SiNPs**, and **7·SiNPs**. (B) Comparison of the XPS Si 2p regions of H−**SiNPs**, **6·SiNPs**, and **7·SiNPs**.

frequencies were noted for **7·SiNPs**, but not H−**SiNPs**. Additionally, it is important to note that some surface oxidation, more pronounced in the case of **7·SiNPs**, was evident from the appearance of a high-frequency shoulder at ∼2231 cm^{-1} in the spectra of both **6·SiNPs** and **7·SiNPs** (Figure 8B,C) and the concomitant growth of a Si−O stretching resonance (centered at 1030−1070 cm^{-1}; see the Supporting Information). The source of and different sensitivity to oxidation are intriguing questions that will be addressed in a subsequent investigation.

^{1}H NMR spectroscopy of the isolated **6·SiNPs** redispersed in C_6D_6 revealed broad resonances in the ranges of 7.8−6.5, 5.8−3.6, 3.7−3.0, and 3.0−0.5 ppm (Figure 9), corresponding to **6·SiNPs**, as well as a set of sharp resonances corresponding to the dihydrogen adduct of **6** (**6**·H_2) formed in ∼6% yield during the treatment of **6**·HCl with LDA (see the Supporting Information). The broad nature of the peaks corresponding to **6**·SiNP is consistent with slowed tumbling of rigid ligands attached to NPs.[66] On the basis of the ^{1}H NMR spectrum of **6**·TTMSS (Figure 4A), the 3.0−0.5 ppm range was assigned to the cyclohexyl, methyl, and methylene protons present in the bound **6**, and the 3.7−3.0 range was assigned to one of the methine protons of the bound **6** (f' in Figure 9). Methine protons f and g, expected to be more downfield (see Figure 4a), were assigned to the broad feature in the range 5.8−3.6 ppm; however, given the relative areas of f' (0.06), f and g were only expected to contribute 0.12 to this feature's total area (1.00); the remainder of the area was assigned to clustered silicon monohydrides (h in Figure 9), based on prior magic-angle spinning (MAS) NMR assignments of similar features[67,68] (notably, no prior reports of solution ^{1}H NMR of fully or partially H-terminated SiNPs could be found). These areas allowed us to make a rough (due to peak overlap and breadth) estimate that 6−7% of the Si−H sites of H−**SiNPs** have been functionalized with **6**. Lastly, the aromatic protons of bound **6** were assigned to the broad peak between 7.8 and 6.5 ppm, which overlapped with the C_6D_5H resonance and a set of sharp resonances from **6**·H_2. These data, in conjunction with the XPS spectroscopy discussed in detail below, were consistent with carbene insertion-functionalization of H−**SiNPs**.

Analysis of the N 1s region of the XPS data for the functionalized NPs, **6**·TTMSS, and protonated carbene precursors offered additional insight into the chemical identity and environment of the bound carbene species (Figure 10A). **6**·TTMSS and **6·SiNP** both displayed a prominent peak with the B.E. of 398.8−398.9 eV (Figure 10A), which was 3.0 eV below the B.E. observed for **6**·HCl (see the Supporting Information). These data provide strong evidence for the insertion of **6** at the H−**SiNP** surface. Similarly, inspection of the XPS N 1s region of **7·SiNPs** (Figure 10A; note: **7**·TTMSS was too volatile to be analyzed via ultrahigh vacuum XPS) revealed a peak with a B.E. of 399.7 eV, ∼0.8 eV higher than for **6·SiNPs** and consistent with the expected aliphatic amines in the monolayer.[18] The absence of a peak at 400.9 eV (N 1s B.E. of **7**·HCl; see the Supporting Information) rules out the presence of the protonated **7** in the **7·SiNPs** sample.

Another salient feature of the N 1s regions for the surfaces, in contrast with **6**·TTMSS, is the 1.3−1.6 times greater full-width half-maximum (fwhm) for the former (Figure 10A), which is consistent with the binding of **6** and **7** to not only the monohydride, but also the di- and trihydride as well as oxidized surface sites. Last, the presence of minor (∼9−12% area) N 1s peak components at higher B.E. for both **6·SiNPs** and **7·SiNPs** (Figure 10A) was ascribed to decomposition during extended Al Kα X-ray irradiation; XPS of **6**·TTMSS for a similar duration resulted in the formation of a new component (∼5% area) at 400.7 eV (Figure S4).

The silicon region of the XPS spectrum was consistent with the ATR-IR results (*vide supra*) in that, as compared to H−**SiNPs**, **6·SiNPs** experienced a moderate increase in the silicon suboxide (SiO_x)[6,63,69,70] component (from 10% in H−**SiNPs** to 25% in isolated **6·SiNPs**), with an increase in its B.E. to 102.7 eV (Figure 10B); **7·SiNP** exhibited a SiO_x peak at 103.0 eV, which constituted 44% of the observed Si 2p signal. Note that the assignment of the higher-B.E. Si 2p peaks to silicon suboxides was supported by comparison to those observed for the H−**SiNP** precursors: 103.4 eV for $(HSiO_{1.5})_n$ and 103.8 eV for SiNPs embedded in a SiO_2 matrix (Figure S5). As mentioned above, the observed oxidation could occur during the course of functionalization or it could be the result of increased SiNP air-sensitivity after carbene functionalization; future studies will seek to further understand this oxidation process with the ultimate goal of controlling it. However, on the basis of the presented spectroscopic evidence, the oxidation is not detrimental to surface functionalization via carbene insertion.

The Si 2p regions had low-intensity and broad but detectable features ∼11 eV higher in B.E. than the Si^0 2p 3/2 peak (see inset in Figure 10B), which were assigned to surface plasmon energy loss.[71] Last, in the carbene-treated SiNP samples, improved fits for the Si 2p region were obtained when a component at 100.8 eV (Figure 10B, green trace) was

DOI: 10.1021/jacs.6b04962
J. Am. Chem. Soc. 2016, 138, 8639−8652

incorporated. This component had greater intensity for **7·SiNPs** as compared to **6·SiNPs** and was proposed to correspond to carbene-bound silicon atoms (Si−C) and low-oxidation state SiO_x.[69] This disparity in the oxidation state of the carbene-functionalized silicon surfaces and the nature of the carbenes likely contributes to the observed differences in SiNP color, dispersibility, and diameter.

IV. Si WAFER STUDIES

Advancing to planar surfaces, we chose to focus on hydrogen-terminated Si(111) wafers (H−**Si(111)**); hydrogen-termination is typically more well-defined for these types of surfaces as compared to Si(100).[6,72] An ideal H−**Si(111)** surface features a regular 2-D array of Si−H bonds positioned normally to the surface at atop silicon sites separated from each other by single tetravalent silicon atoms. XPS analysis of these wafers and submonolayer silicon oxide quantification following the method introduced by Lewis and Haber[73] confirmed that the content of the oxidized atop silicon sites was generally low (0−9% with an average of ∼5% for all of the tested batches of etched wafers; see Figure S6 for several examples).

Freshly etched wafers were exposed to a 0.048 M solution of **6** in C_6D_6 at 23 °C, as in the model studies. The insertion process for wafers was monitored by XPS. On the basis of the relative nitrogen content and substrate-overlayer model analysis (see the Supporting Information), the coverage of Si(111) atop sites by **6** (Φ_6) was found to have reached 12 ± 1% after a 10 min exposure and saturated at 21 ± 3% after 3 days (Figure 11A). This saturation coverage implies that 21 ± 3% of the surface Si−H bonds reacted with **6**, and it is consistent with the maximal coverage of Si(111) atop sites (∼20%) expected from computed structures of **6** bound to atomically rough surface models (*vide infra*).

In the case of **7**, the wafers were rinsed for ∼20 s with Milli-Q water prior to analysis to remove physisorbed lithium-, chlorine-, and nitrogen-containing species, as confirmed by XPS. For the 20 min and 4 h treatment times, virtually identical Φ_7 was seen: 9 ± 1% (Figure 11A). This relatively low coverage as compared to the expected maximum ≥25% (based on computed surface, *vide infra*) is hypothesized to result from competitive physisorption of the species described above, as well as competitive dimerization of **7**.

Similarly to **6**·TTMSS and **6·SiNP**, the N 1s region of **6·Si(111)** XPS data exhibited a peak at a B.E. of 398.8 eV, consistent with the insertion of **6** at the H−**Si(111)** surface (Figure 11B). Likewise, the N 1s region for **7·Si(111)** had a peak at 399.7 eV, which is identical to the value observed for **7·SiNPs**. The fwhm values observed for Si wafers were also approximately the same as those for SiNPs, which suggested that the carbenes were binding to different surface sites (*vide infra*). The additional component (∼20% of the peak area, Figure 11B) at 400.4 eV in the N 1s region of **6·Si(111)** could arise, as in the case of **6·SiNPs**, through X-ray-induced decomposition. Aqueous wash did not eliminate this component or significantly alter Φ_N (∼5% change), but instead resulted in additional silicon surface oxidation (see Figure S7A), with concomitant shift of the N 1s peak by +0.2−0.3 eV and increase in fwhm by ∼64% (see Figure S7B), which supported the proposed origin of the high-B.E. component and the elevated fwhm. The N 1s region of the **7·Si(111)** (rinsed with H_2O) also exhibited a minor peak component at 402.4 eV (Figure 11B), which is nearly identical to what has been previously noted for polyethylenimine-ethoxylated (PEIE)

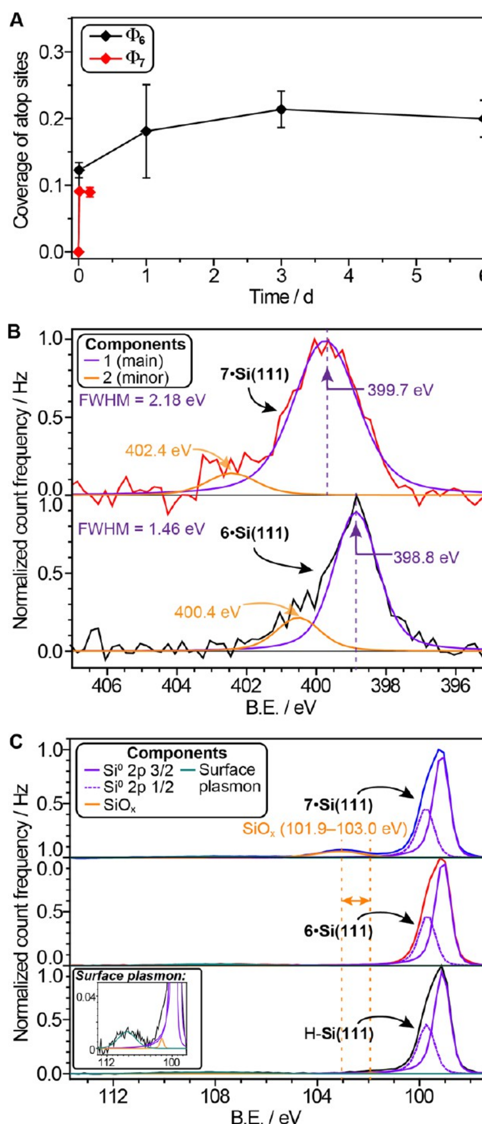

Figure 11. (A) Carbene coverage of **Si(111)** by carbenes **6** and **7** from XPS. For all time points, averages were determined from ≥4 values, except the 10 min time point for **6** and 20 min time point for **7** (2 values for each). Error bars represent standard deviations. (B) N 1s regions for **6·Si(111)** and **7·Si(111)**. (C) Si 2p regions for H−**Si(111)**, **6·Si(111)**, and **7·Si(111)**.

(sub)monolayers deposited from pH = 7 solutions or rinsed with H_2O (pH = 7).[18] The component at 402.4 eV was assigned, by analogy with PEIE, to the protonated (or H-bonded to H_2O) amine groups.[18] Finally, analysis of the Si 2p region (Figure 11C) revealed that **7·Si(111)**, like **7·SiNPs**, experienced substantial (72% SiO_x) surface oxidation, while treatment with **6** had virtually no effect on the state of oxidation of the **Si(111)** wafers. Collectively, the XPS data are qualitatively consistent with the data obtained for SiNPs; they strongly support the expected structure of the monolayers derived from carbene insertion into surface Si−H bonds.

Transmission FTIR spectroscopy of H−**Si(111)** wafers treated with **6** and **7** (Figure 12) also indicated structural correspondence between the planar surfaces, SiNPs, and the model compounds in this study. IR spectra were acquired for two separate samples reacted with each carbene; while there were small differences between samples in the total amount of surface functionalization, the resulting spectra were qualitatively

DOI: 10.1021/jacs.6b04962
J. Am. Chem. Soc. 2016, 138, 8639−8652

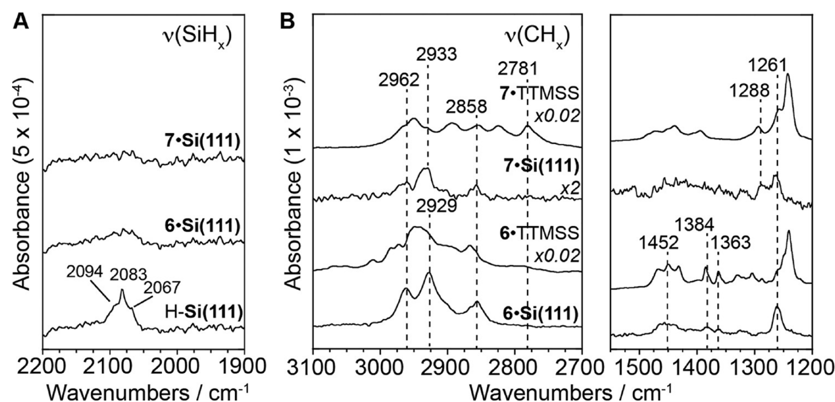

Figure 12. Transmission FTIR spectra of (A) the Si−H stretch region of untreated and carbene-treated H−**Si(111)** wafers, ratioed to a fully oxidized (SiH_x-free) Si(111) surface, and (B) the 3500−2500 and 1650−1250 cm^{-1} regions of the carbene-treated H−**S(111)** wafers, ratioed to the untreated surface, as compared to the corresponding TTMSS−carbene adducts.

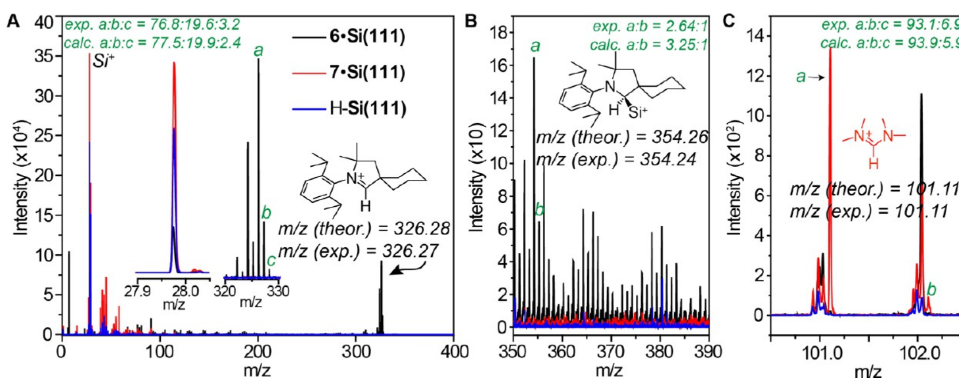

Figure 13. (A) TOF-SIMS spectra (m/z = 0−400 Da) of H−**Si(111)** surfaces before and after functionalization with **6** and **7** (insets zoom in on Si^+ and 6·H^+ ions peaks). (B) TOF-SIMS spectra zoomed in on the region where peaks corresponding to Si-bound **6** ions may be found. (C) TOF-SIMS spectra zoomed in on the region where peaks corresponding to the **7**·H^+ ions may be found.

the same. It is important to note at the outset that the spectrum of the initial H−**Si(111)** surface in Figure 12A demonstrates that our surface had significant atomic roughness[74,75] as compared to the ideal monohydride-terminated Si(111) surface. The sharp peak at the center of the SiH stretching band (2083 cm^{-1}) arises from monohydride terraces, while the prominent shoulders at ∼2067 and ∼2094 cm^{-1} correspond to coupled step monohydride (M) defects (symmetric and asymmetric vibrations, respectively). The higher-frequency tail extending out to ∼2150 cm^{-1} is likely due to dihydride (D) and trihydride (Tr) defects.[74,75] We were unable to definitively rule out higher-frequency peaks corresponding to minority $(SiO)_3SiH$ species due to the presence of an N_2O resonance in the same region from a small amount of impurity in the spectrometer purge gas; however, no significant Si−O stretching peaks were detected on the untreated H−**Si(111)** wafers.

Integration of the Si−H stretching signal from carbene-treated H−**Si(111)** wafers gave an estimated 36% conversion of the Si−H bonds upon reaction with **6** and 70% conversion upon reaction with **7**; these conversion values represent a combination of carbene insertion and silicon oxidation reactions. As is evident in Figure 12A, the initially sharp $\nu(SiH_x)$ bands broaden considerably after reaction with the carbenes, which renders integration of this peak, and therefore the calculated Si−H conversion, sensitive to small variations in the baseline; these values should therefore be considered as rough estimates. Additionally, some surface oxidation was observed for both **6**·**Si(111)** and **7**·**Si(111)**, which likely accounts for some of the decrease in surface SiH_x species by replacement with surface SiOH or $(SiO)_3SiH$ species.[76] The extent of surface oxidation, estimated by integration of the Si−O stretching bands in the two samples of each reaction type at ∼1000−1150 cm^{-1} (see the Supporting Information) and comparison with the intensity of the SiO_2 phonon signal from a chemical oxide, ranged from 28% to 33% of a full oxide layer after reaction with **7** and from 5% to 24% of a full layer after reaction with **6**. These values are qualitatively consistent with the extent of oxidation determined by XPS.

The spectra in Figure 12B illustrate the changes in vibrational modes upon treatment of H−**Si(111)** with **6** and **7** and draw a comparison with the TTMSS adducts of both carbenes. Thus, spectra of both **6**·**Si(111)** and **6**·TTMSS display a band between 1415 and 1490 cm^{-1} (centered at ∼1452 cm^{-1}), as well as the peaks at 1384 and 1363 cm^{-1}, which, guided by density functional theory (DFT) computations (see the Supporting Information) and literature,[77] have been assigned as follows: 1415−1490 cm^{-1} to CH_3 and CH_2 asymmetric deformation vibrations, and 1363 and 1384 cm^{-1} to $CH(CH_3)_2$ or $C(CH_3)_2$ fragment symmetric deformation vibrations. On the other hand, **7**·**Si(111)** and **7**·TTMSS both display a resonance at ∼1288 cm^{-1}, assigned to a "wagging" vibration mode spanning multiple C−H and C−N bonds in **7** (Figure 12B). These features map well onto those observed for the corresponding SiNP samples (Figure 8).

DOI: 10.1021/jacs.6b04962
J. Am. Chem. Soc. 2016, 138, 8639−8652

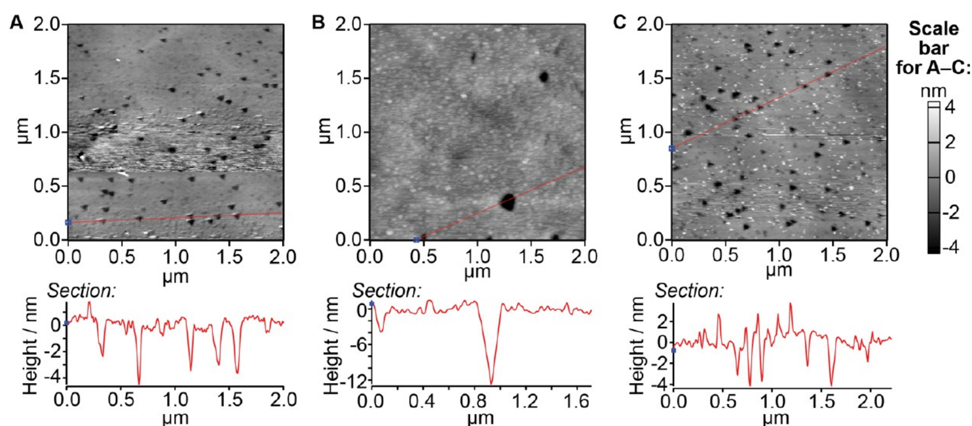

Figure 14. Representative tapping-mode AFM height retraces for (A) an H−Si(111) wafer, (B) a **6**·Si(111) wafer rinsed with Milli-Q water for ∼30 s, and (C) a 7·Si(111) wafer rinsed with Milli-Q water for ∼30 s, derived from the same batch of etched wafers. The red line in the images indicates the cross-sections, from which the height plots below the AFM images were generated.

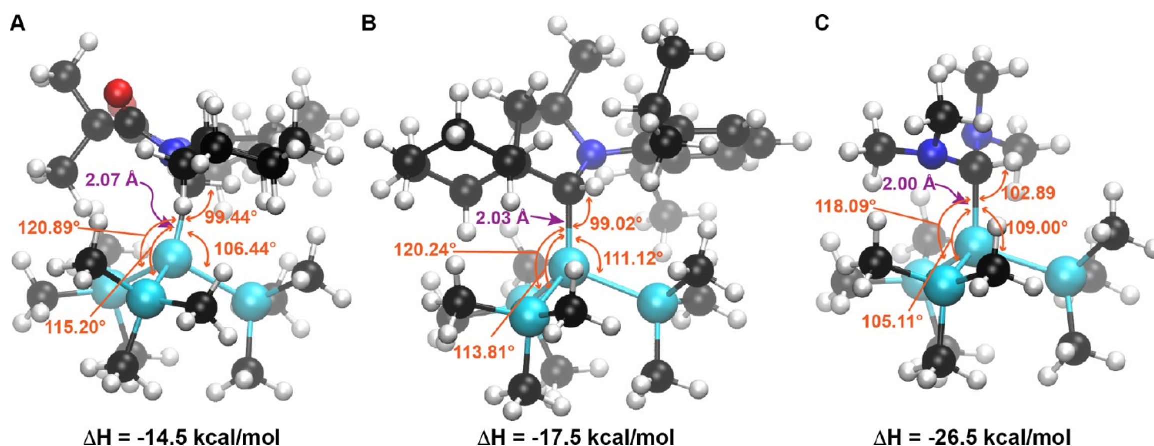

Figure 15. (A−C) Computed energy-minimized structures (represented as ball-and-stick models) of **5**·TTMSS (A), **6**·TTMSS (B), and 7·TTMSS (C). Hydrogen atoms are in white, carbon in black, nitrogen in blue, oxygen in red, and silicon in cyan.

The C−H stretch regions of the IR spectra of **6**·TTMSS and **7**·TTMSS were also quite similar to those of **6**·**SiNPs** and 7·**SiNPs**, respectively. The spectrum of 7·TTMSS displayed a resonance at 2781 cm^{-1} not present in the spectrum of **6**·TTMSS, while the latter alone had a low-intensity peak between 3034 and 3069 cm^{-1} corresponding to aromatic C−H stretches. DFT computation of the vibration frequencies of 7·TTMSS indicated that, as expected,[77] the aminal C−H bond stretch has the lowest stretching frequency of the C−H bonds in the molecule, 2809 cm^{-1}. Given that overestimation by, on average, 30−50 cm^{-1} is typical for DFT computations of vibrational frequencies using the PBE functional,[78,79] this value is in excellent agreement with the observed resonances at 2781 cm^{-1} (2770 cm^{-1} in SiNPs). Although these weak "marker" C−H stretch resonances were difficult to discern in the spectra of **6**·**Si(111)** and 7·**Si(111)**, differences in relative peak intensities in the C−H stretch region for these two sets of samples are consistent with the disparity in their monolayer composition.

To complement the spectroscopic data for the Si(111) wafers, time-of-flight secondary ion mass spectrometry (TOF-SIMS) was carried out on a set of wafers before and after carbene treatment. Analysis of **6**·**Si(111)** wafers revealed a new dominant peak at m/z = 326.27 Da (Figure 13A), which corresponds within 52 ppm (and with an identical isotope pattern) to **6**·H^+. A weaker signal at 354.24 was also observed, which was consistent (within 62 ppm) with **6**·$H(Si)^+$ (Figure 13B). C−Si fragmentation to yield 6·H^+ was similarly dominant in the FTICR-MS of the **6**·TTMSS adduct (see the Supporting Information). TOF-SIMS of 7·**Si(111)** likewise revealed an ion peak that was unique to this surface among the three tested (Figure 13C): the ion with m/z = 101.11 and the isotope pattern corresponded well with the theoretical values for 7·H^+. In conjunction with the spectroscopic evidence above, these TOF-SIMS data strongly support the structural assignments of the carbene Si−H insertion-derived monolayers.

Last, the surface morphology was inspected for the Si(111) wafers before and after exposure to carbenes. As anticipated from the analysis of IR spectra (vide supra), nanoscopic surface roughness was observed by tapping-mode atomic force microscopy (AFM), which revealed an abundance of triangular etch pits of various lateral cross sections (∼70−160 nm) and depths (1−5 nm) (Figure 14A). Such features have previously been demonstrated to result from the presence of dissolved oxygen in aqueous etchants.[80,81] Inspection of the AFM height retraces for **6**·**Si(111)** and 7·**Si(111)**, both briefly rinsed with water, revealed clear morphological differences between these surfaces and also in comparison with H−**Si(111)** (Figure 14B,C). Specifically, while the density and size of "triangular" pits in 7·**Si(111)** were roughly the same as in H−**Si(111)**, **6**·**Si(111)** exhibited fewer but larger ones (e.g., the ∼12 nm deep and ∼200 nm wide pit in Figure 14B). On the other hand, 7·**Si(111)** appeared to have a much higher density of small

DOI: 10.1021/jacs.6b04962
J. Am. Chem. Soc. 2016, 138, 8639−8652

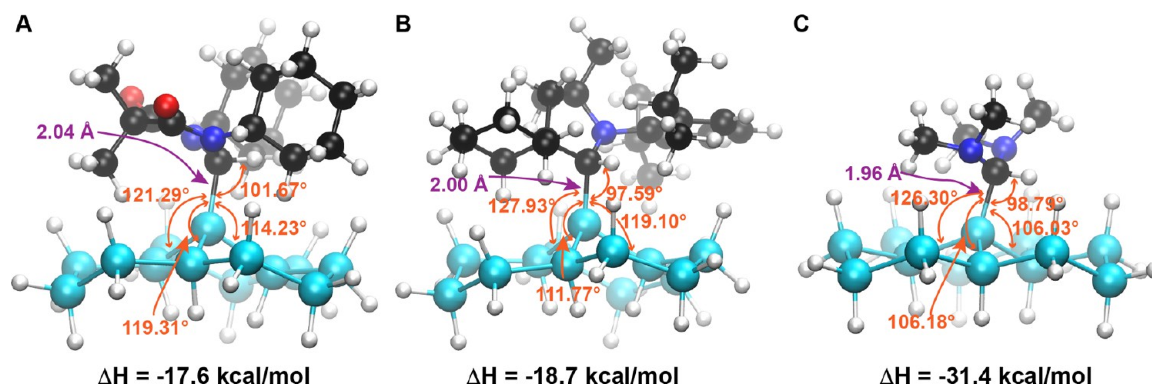

Figure 16. (A–C) Computed energy-minimized structures (represented as ball-and-stick models) of insertion products of **5** (A), **6** (B), and **7** (C) into the central Si–H bond of a 13-Si-atom, one-layer H–**Si(111)** surface model. Hydrogen atoms are in white, carbon in black, nitrogen in blue, oxygen in red, and silicon in cyan.

elevated features as compared to the other two. The origin of these morphological differences could stem from a combination of surface functionalization with carbenes as well as surface oxidation, as noted earlier.

V. COMPUTATIONAL STUDIES

To gain more insight into the thermodynamics of insertion of **6** and **7** into the Si–H bonds of TTMSS, TTMSOxS, and H–**Si** surfaces, as well as into the geometry of the resultant monolayers, we set out to investigate these systems computationally. As a valuable point of comparison, we also included **5** and its analogous insertion products in this study. We employed density functional theory (DFT) with the PBE functional[82] and 6-311g** basis set to model the structures, similarly to previous studies of organic monolayers on Si(111).[83,84]

Comparing the TTMSS adducts, we find that for all three carbenes, the enthalpy change (Δ*H*) for the Si–H insertion is moderate in magnitude and negative (Figure 15A–C), consistent with the experimentally observed insertion reactivity. The Δ*H* appears to be positively correlated with the $Si-C_{carbene}$ bond length and is greatest in magnitude for carbene **7** (−26.5 kcal/mol), for which this bond length is the shortest (2.00 Å). Notably, the $C_{carbene}$–Si bond lengths and the proximal $Si-C_{carbene}-H$ bond angles for all structures both show sizable deviations from what might be expected for a $Si_{sp^3}-C_{sp^3}$ system (1.86 Å[85] and 109.5°, respectively). Furthermore, one of the three $Si-Si-C_{carbene}$ bond angles in each molecule is expanded to ∼118–121°, which is due to the inclination of the $Si-C_{carbene}$ bond relative to the normal of the plane spanned by the "peripheral" Si atoms", most evident in Figure 15A.

We find a very similar pattern in the crystal structure of **6**·TTMSS (Figure 4C): the $Si-Si-C_{carbene}$ angles are equal to within 1.5°, and although the $Si-C_{carbene}$ bond length is 0.05 Å shorter (at 1.98 Å), and the $Si-C_{carbene}-H$ bond angle is slightly larger (104.9°), the difference of which can be attributed to the self-interaction error inherent in DFT calculations, these results point to substantial steric interaction between the carbene- and TTMSS-derived portions of the molecules, which induces the observed structural distortions. Such distortions have previously been observed in bis(hypersilyl)methane, which has a similar steric bulk relationship between a tris(trimethylsilyl)silyl (i.e., hypersilyl) group and another molecular fragment attached to it.[86]

Extending these computations to surfaces, we designed a one-layer 13-Si-atom model of a H–**Si(111)** surface, for which the valence of all silicon atoms was fulfilled via appended hydrogen atoms (Figure 16A–C). This particular model was selected because it is the minimal such surface whose size is large enough to span carbenes **5**–**7**, and thereby take steric effects between the carbene and the silicon surface into account. The computed Δ*H* values were slightly greater in magnitude for the Si_{13} model (1.2–4.9 kcal/mol) than in corresponding TTMSS adducts, and, accordingly, the $Si-C_{carbene}$ bond lengths were slightly shorter, although the "tilt" of the $Si-C_{carbene}$ bond was still pronounced. A new feature that was not evident in the TTMSS adducts was the buckling of the silicon surface, which was absent in the case of **7**, but noticeable in the case of **5** and **6**, the more sterically demanding carbenes. This buckling presumably alleviates that steric strain that would otherwise be present.

To evaluate the likelihood that such a deformation might take place at a real, rigid silicon surface, we constructed a three-layer silicon model to test the insertion of **6**, a more sterically demanding carbene, and **7**, a less sterically encumbered one. The geometry of the three-layer model with no molecular adduct was allowed to relax; then, the bottom two layers of atoms were frozen in place, and the molecules **6** and **7** were inserted into the Si–H bond. The geometries of the top layer of the surface model plus the organic molecule were allowed to relax, with the bottom two layers held fixed at their vacuum-optimized geometry (Figure 17). In this case, the computed Δ*H* was moderate and positive for **6**, indicating that a perfectly flat H-terminated silicon surface is unlikely to participate in insertion reactions with **6** (Figure 17A). The analogous three-layer model for **7** produced results virtually identical to those of the one-layer model (Figure 17B).

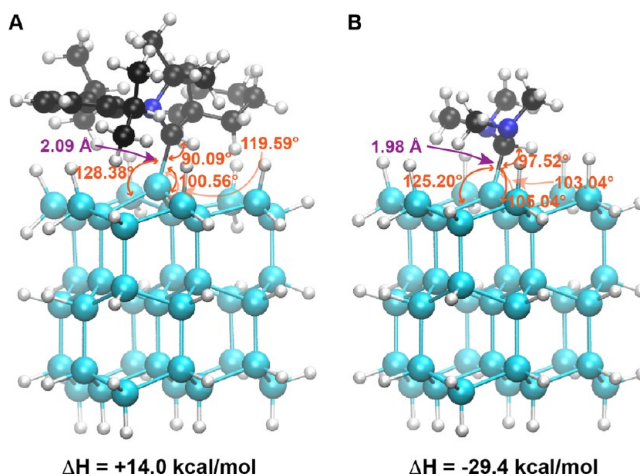

Figure 17. (A,B) Computed energy-minimized structures (represented as ball-and-stick models) of insertion products of **6** (A) and **7** (B) into the central Si–H bond of a 39-Si-atom, three-layer H–**Si(111)** surface model. Hydrogen atoms are in white, carbon in black, nitrogen in blue, and silicon in cyan.

As was described above, our H-**Si(111)** surfaces, and certainly the H-**SiNP** surfaces, were not flat and possessed numerous defects both at the atomic level and at the nanoscale; also, the binding of both **6** and **7** was observed for these surfaces, with all evidence suggesting that insertion, indeed, took place. Thus, based on our calculations we conclude that, while **7** (and **5**) can, in principle, bind to flat regions, **6** likely binds to the defect sites. Defects discussed earlier, D, Tr, M, and

DOI: 10.1021/jacs.6b04962
J. Am. Chem. Soc. 2016, 138, 8639–8652

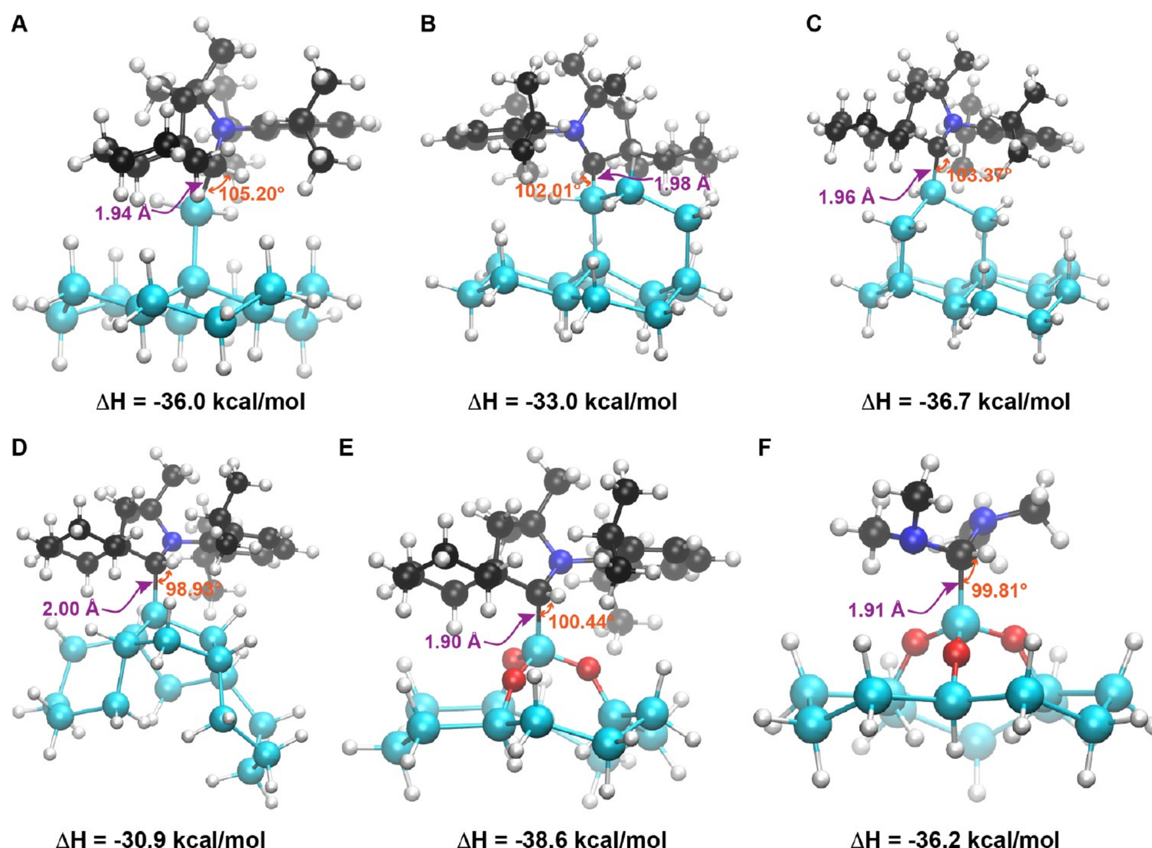

Figure 18. (A–F) Computed energy-minimized structures (represented as ball-and-stick models) of insertion products of **6** with the following surface defects: Tr (A), two sets of variants of D (B,C), M (D), and $(SiO)_3SiH$ (E). The latter is also computed for carbene **7** (F). The 13-Si atom base layer was the same as used for the calculations presented in Figure 16; silicon atoms were displaced from this base layer, and additional oxygen and silicon atoms were included in the surface model, as needed to form the defects studied. Hydrogen atoms are in white, carbon in black, nitrogen in blue, oxygen in red, and silicon in cyan.

$(SiO)_3SiH$, were thus incorporated onto the one-layer surface, and the insertion of **6** and **7** was examined (Figure 18A–F).

The results revealed that in all of the cases that were explored, binding of **6** to the defects was highly thermodynamically favorable, and the resulting Si–$C_{carbene}$ bond length continued to decrease with increased magnitude of ΔH. The greatest magnitude of ΔH (−38.6 kcal/mol) was seen for insertion of **6** at the oxidized silicon (i.e., $(SiO)_3SiH$), accompanied by the shortest Si–$C_{carbene}$ bond length of 1.90 Å. Insertion of **7** was tested only on the latter substrate, and this process was nearly equally thermodynamically favorable. Hence, these results support the notion that **6** inserts primarily into the "more exposed" Si–H bonds of silicon surfaces, while **7** is perhaps less selective.

VI. CONCLUSIONS

Herein, we demonstrated the use of persistent carbenes for functionalization of hydrogen-terminated silicon surfaces. Model compounds, SiNPs, and Si(111) wafers were used as substrates to investigate carbene reactivity with Si–H bonds. Through the use of a combination of characterization techniques, several valuable insights were gained that will aide the future development of carbene-derived monolayers. (1) We found that both enhanced nucleophilicity and electrophilicity (e.g., in CAACs and ADACs) as well as reduced or flexible steric bulk of the persistent carbene were necessary to achieve rapid Si–H insertion reactivity. (2) The reaction of CAAC **6** with Si(111) surfaces proceeds cleanly at room temperature and is complete within 3 days at concentrations as low as 0.048 M, having reached expected coverage of ∼21 ± 3%, while in the case of **7**, which was plagued by decomposition, saturation is observed after 20 min, with carbene coverage of 9 ± 1%, and significant concomitant oxidation of the surface. (3) Both carbenes appear to bind to a range of surface sites (e.g., terrace Si–H and defects M, D, Tr, and oxidized surface sites); in fact, reaction with the defects is thermodynamically favored for the sterically more encumbered carbene **6**. Thus, we anticipate that **6** may be well-suited for the functionalization of hydrogen-terminated Si(100) surfaces. (4) CAAC **6**, due to its large steric bulk, leaves unreacted Si–H bonds at the surface of both Si(111) wafers and SiNPs, which could prove valuable for silicon patterning. (5) Last, the fact that redispersible SiNPs with unreacted Si–H functionality can be obtained by functionalization with carbene **6** indicates that CAAC-type carbenes could, with optimization, deliver stable SiNPs with previously inaccessible physicochemical properties.

■ ASSOCIATED CONTENT

Supporting Information

The Supporting Information is available free of charge on the ACS Publications website at DOI: 10.1021/jacs.6b04962.

Materials and methods, detailed synthetic and characterization procedures, supplementary figures, and spectral data (PDF) (PDF)

X-ray crystallographic data for **6**·TTMSS (CIF)

X-ray crystallographic data for $(\mathbf{5})_2$ (CIF)

X-ray crystallographic data for **6**·HCl (CIF)

X-ray crystallographic data for **4**·HOTf (CIF)

DOI: 10.1021/jacs.6b04962
J. Am. Chem. Soc. 2016, 138, 8639–8652

X-ray crystallographic data for **5**·HOTf (CIF)

AUTHOR INFORMATION

Corresponding Author

*jaj2109@mit.edu

Notes

The authors declare the following competing financial interest(s): A patent has been filed on this surface modification process.

ACKNOWLEDGMENTS

We thank the National Science Foundation (CHE-1334703 and CHE-1351646) and the DoD NDSEG and Intel (graduate fellowships for A.V.Z.) for support of this work. We thank Dr. P. Clark for TOF-SIMS acquisition, Dr. Li Li for FTICR-MS data acquisition, Dr. Y. Zhang for help with TEM imaging, Dr. A. Schwartzman for help with AFM imaging, and Dr. P. Müller for X-ray crystallography. We are also grateful to Dr. J. Simpson for assistance with 2D NMR spectroscopy, M. Campion for assistance with the furnace setup for SiNP fabrication, and Prof. T. Swager for the use of his group's ATR-FTIR spectrometer. Last, we are indebted to Dr. N. Fairley for invaluable discussion of XPS analysis. This work made use of the MRSEC Shared Experimental Facilities supported by the National Science Foundation under award number DMR-1419807, as well as the DCIF facility NMR instruments supported by NIH Grant no. 1S10RR013886-01 and NSF grant no. DBI-9729592.

REFERENCES

(1) Balani, K.; Verma, V.; Agarwal, A.; Narayan, R. *Biosurfaces: A Materials Science and Engineering Perspective*; John Wiley & Sons, Inc.: Hoboken, NJ, 2015.
(2) Bhushan, B. *Principles and Applications of Tribology*, 2nd ed.; John Wiley & Sons, Ltd.: New York, 2013.
(3) Birdi, K. S. *Surface Chemistry Essentials*; CRC Press: Boca Raton, FL, 2013.
(4) Brillson, L. J. *Surfaces and Interfaces of Electronic Materials*; Wiley-VCH: Weinheim, 2010.
(5) *Functional Surfaces in Biology: Little Structures with Big Effects*; Springer: Netherlands, 2009; Vol. *1*.
(6) Higashi, G. S.; Chabal, Y. J. In *Handbook of Semiconductor Wafer Cleaning Technology*; Kern, W., Ed.; Noyes Publication: NJ, 1993; p 433.
(7) Kaminski, P. M.; Abbas, A.; Bass, K.; Claudio, G. *Energy Procedia* **2011**, *10*, 71.
(8) Hofmann, M.; Janz, S.; Schmidt, C.; Kambor, S.; Suwito, D.; Kohn, N.; Rentsch, J.; Preu, R.; Glunz, S. W. *Sol. Energy Mater. Sol. Cells* **2009**, *93*, 1074.
(9) Ferre, R.; Martín, I.; Vetter, M.; Garín, M.; Alcubilla, R. *Appl. Phys. Lett.* **2005**, *87*, 202109.
(10) Webb, L. J.; Lewis, N. S. *J. Phys. Chem. B* **2003**, *107*, 5404.
(11) Bansal, A.; Li, X.; Lauermann, I.; Lewis, N. S.; Yi, S. I.; Weinberg, W. H. *J. Am. Chem. Soc.* **1996**, *118*, 7225.
(12) Linford, M. R.; Fenter, P.; Eisenberger, P. M.; Chidsey, C. E. D. *J. Am. Chem. Soc.* **1995**, *117*, 3145.
(13) Linford, M. R.; Chidsey, C. E. D. *J. Am. Chem. Soc.* **1993**, *115*, 12631.
(14) Green, M. L.; Gusev, E. P.; Degraeve, R.; Garfunkel, E. L. *J. Appl. Phys.* **2001**, *90*, 2057.
(15) Aberle, A. G. *Prog. Photovoltaics* **2000**, *8*, 473.
(16) DeBenedetti, W. J. I.; Chabal, Y. J. *J. Vac. Sci. Technol., A* **2013**, *31*, 050826.
(17) Sieval, A. B.; Linke, R.; Heij, G.; Meijer, G.; Zuilhof, H.; Sudhölter, E. J. R. *Langmuir* **2001**, *17*, 7554.
(18) Zhou, Y.; Fuentes-Hernandez, C.; Shim, J.; Meyer, J.; Giordano, A. J.; Li, H.; Winget, P.; Papadopoulos, T.; Cheun, H.; Kim, J.; Fenoll, M.; Dindar, A.; Haske, W.; Najafabadi, E.; Khan, T. M.; Sojoudi, H.; Barlow, S.; Graham, S.; Brédas, J.-L.; Marder, S. R.; Kahn, A.; Kippelen, B. *Science* **2012**, *336*, 327.
(19) Malyar, I. V.; Gorin, D. A.; Stetsyura, S. V.; Santer, S. *J. Electron. Mater.* **2012**, *41*, 3427.
(20) Ahlbrecht, H. *Encyclopedia of Reagents for Organic Synthesis*; John Wiley & Sons, Ltd.: New York, 2001.
(21) Zhukhovitskiy, A. V.; MacLeod, M. J.; Johnson, J. A. *Chem. Rev.* **2015**, *115*, 11503.
(22) Hopkinson, M. N.; Richter, C.; Schedler, M.; Glorius, F. *Nature* **2014**, *510*, 485.
(23) Liu, W.; Sharp, I. D.; Tilley, T. D. *Langmuir* **2014**, *30*, 172.
(24) Saghatelian, A.; Buriak, J.; Lin, V. S. Y.; Reza Ghadiri, M. *Tetrahedron* **2001**, *57*, 5131.
(25) Aslanov, L.; Zakharov, V.; Zakharov, M.; Kamyshny, A.; Magdassi, S.; Yatsenko, A. *Russ. J. Coord. Chem.* **2010**, *36*, 330.
(26) Frey, G. D.; Masuda, J. D.; Donnadieu, B.; Bertrand, G. *Angew. Chem., Int. Ed.* **2010**, *49*, 9444.
(27) Schmidt, D.; Berthel, J. H. J.; Pietsch, S.; Radius, U. *Angew. Chem., Int. Ed.* **2012**, *51*, 8881.
(28) Lastovickova, D. N.; Moerdyk, J. P.; Kelley, A. R.; Bielawski, C. W. *J. Phys. Org. Chem.* **2015**, *28*, 75.
(29) Zhukhovitskiy, A. V.; Mavros, M. G.; Van Voorhis, T.; Johnson, J. A. *J. Am. Chem. Soc.* **2013**, *135*, 7418.
(30) MacLeod, M. J.; Johnson, J. A. *J. Am. Chem. Soc.* **2015**, *137*, 7974.
(31) Chatgilialoglu, C.; Lalevée, J. *Molecules* **2012**, *17*, 527.
(32) Zhukhovitskiy, A. V.; Geng, J.; Johnson, J. A. *Chem. - Eur. J.* **2015**, *21*, 5685.
(33) Denk, M. K.; Thadani, A.; Hatano, K.; Lough, A. J. *Angew. Chem., Int. Ed. Engl.* **1997**, *36*, 2607.
(34) Alder, R. W.; Blake, M. E.; Chaker, L.; Harvey, J. N.; Paolini, F.; Schütz, J. *Angew. Chem., Int. Ed.* **2004**, *43*, 5896.
(35) César, V.; Lugan, N.; Lavigne, G. *Eur. J. Inorg. Chem.* **2010**, *2010*, 361.
(36) Hudnall, T. W.; Bielawski, C. W. *J. Am. Chem. Soc.* **2009**, *131*, 16039.
(37) Chen, M.; Moerdyk, J. P.; Blake, G. A.; Bielawski, C. W.; Lee, J. K. *J. Org. Chem.* **2013**, *78*, 10452.
(38) César, V.; Lugan, N.; Lavigne, G. *J. Am. Chem. Soc.* **2008**, *130*, 11286.
(39) Moerdyk, J. P.; Bielawski, C. W. *Chem. - Eur. J.* **2013**, *19*, 14773.
(40) Altenhoff, G.; Goddard, R.; Lehmann, C. W.; Glorius, F. *J. Am. Chem. Soc.* **2004**, *126*, 15195.
(41) Altenhoff, G.; Goddard, R.; Lehmann, C. W.; Glorius, F. *Angew. Chem., Int. Ed.* **2003**, *42*, 3690.
(42) Moerdyk, J. P.; Bielawski, C. W. *Chem. Commun. (Cambridge, U. K.)* **2014**, *50*, 4551.
(43) Moerdyk, J. P.; Blake, G. A.; Chase, D. T.; Bielawski, C. W. *J. Am. Chem. Soc.* **2013**, *135*, 18798.
(44) Martin, D.; Lassauque, N.; Donnadieu, B.; Bertrand, G. *Angew. Chem., Int. Ed.* **2012**, *51*, 6172.
(45) Hudnall, T. W.; Moerdyk, J. P.; Bielawski, C. W. *Chem. Commun. (Cambridge, U. K.)* **2010**, *46*, 4288.
(46) Frey, G. D.; Lavallo, V.; Donnadieu, B.; Schoeller, W. W.; Bertrand, G. *Science* **2007**, *316*, 439.
(47) Lloyd-Jones, G. C.; Alder, R. W.; Owen-Smith, G. J. J. *Chem. - Eur. J.* **2006**, *12*, 5361.
(48) Allen, F. H.; Kennard, O.; Watson, D. G.; Brammer, L.; Orpen, A. G.; Taylor, R. *J. Chem. Soc., Perkin Trans. 2* **1987**, S1.
(49) Soleilhavoup, M.; Bertrand, G. *Acc. Chem. Res.* **2015**, *48*, 256.
(50) Melaimi, M.; Soleilhavoup, M.; Bertrand, G. *Angew. Chem., Int. Ed.* **2010**, *49*, 8810.
(51) Zeng, X.; Frey, G. D.; Kinjo, R.; Donnadieu, B.; Bertrand, G. *J. Am. Chem. Soc.* **2009**, *131*, 8690.
(52) Jazzar, R.; Dewhurst, R. D.; Bourg, J.-B.; Donnadieu, B.; Canac, Y.; Bertrand, G. *Angew. Chem., Int. Ed.* **2007**, *46*, 2899.

DOI: 10.1021/jacs.6b04962
J. Am. Chem. Soc. 2016, 138, 8639−8652

(53) Jazzar, R.; Bourg, J.-B.; Dewhurst, R. D.; Donnadieu, B.; Bertrand, G. *J. Org. Chem.* **2007**, *72*, 3492.
(54) Lavallo, V.; Canac, Y.; Präsang, C.; Donnadieu, B.; Bertrand, G. *Angew. Chem., Int. Ed.* **2005**, *44*, 5705.
(55) Martin, D.; Canac, Y.; Lavallo, V.; Bertrand, G. *J. Am. Chem. Soc.* **2014**, *136*, 5023.
(56) W. Alder, R.; E. Blake, M.; Bortolotti, C.; Bufali, S.; P. Butts, C.; Linehan, E.; M. Oliva, J.; Guy Orpen, A.; J. Quayle, M. *Chem. Commun.* **1999**, 241.
(57) Alder, R. W.; Blake, M. E.; Oliva, J. M. *J. Phys. Chem. A* **1999**, *103*, 11200.
(58) Bell, J. P.; Cloud, J. E.; Cheng, J.; Ngo, C.; Kodambaka, S.; Sellinger, A.; Ratanathanawongs Williams, S. K.; Yang, Y. *RSC Adv.* **2014**, *4*, 51105.
(59) Mastronardi, M. L.; Maier-Flaig, F.; Faulkner, D.; Henderson, E. J.; Kübel, C.; Lemmer, U.; Ozin, G. A. *Nano Lett.* **2012**, *12*, 337.
(60) Veinot, J. G. C. *Chem. Commun.* **2006**, 4160.
(61) Hessel, C. M.; Henderson, E. J.; Veinot, J. G. *Chem. Mater.* **2006**, *18*, 6139.
(62) Dasog, M.; Yang, Z.; Regli, S.; Atkins, T. M.; Faramus, A.; Singh, M. P.; Muthuswamy, E.; Kauzlarich, S. M.; Tilley, R. D.; Veinot, J. G. C. *ACS Nano* **2013**, *7*, 2676.
(63) Niwano, M.; Kageyama, J. i.; Kurita, K.; Kinashi, K.; Takahashi, I.; Miyamoto, N. *J. Appl. Phys.* **1994**, *76*, 2157.
(64) Ling, X.; Roland, S.; Pileni, M.-P. *Chem. Mater.* **2015**, *27*, 414.
(65) Vignolle, J.; Tilley, T. D. *Chem. Commun.* **2009**, 7230.
(66) Copéret, C.; Chaudret, B. *Surface and Interfacial Organometallic Chemistry and Catalysis*; Springer Verlag: Germany, 2005.
(67) Neiner, D.; Kauzlarich, S. M. *Chem. Mater.* **2010**, *22*, 487.
(68) Onischuk, A. A.; Strunin, V. P.; Samoilova, R. I.; Nosov, A. V.; Ushakova, M. A.; Panfilov, V. N. *J. Aerosol Sci.* **1997**, *28*, 1425.
(69) Yang, Z.; Gonzalez, C. M.; Purkait, T. K.; Iqbal, M.; Meldrum, A.; Veinot, J. G. C. *Langmuir* **2015**, *31*, 10540.
(70) Tufts, B. J.; Kumar, A.; Bansal, A.; Lewis, N. S. *J. Phys. Chem.* **1992**, *96*, 4581.
(71) Erickson, N. E.; Lieberman, A. G.; Madey, T. E.; Yates, J. T., Jr. In *Semiconductor Measurement Technology: Progress Report, January 1 to June 30, 1976*; Bullis, W. M., Ed.; U.S. Dept. of Commerce, National Bureau of Standards: Washington, DC, 1976; Vol. *400*, p 28.
(72) Higashi, G. S.; Chabal, Y. J.; Trucks, G. W.; Raghavachari, K. *Appl. Phys. Lett.* **1990**, *56*, 656.
(73) Haber, J. A.; Lewis, N. S. *J. Phys. Chem. B* **2002**, *106*, 3639.
(74) Garcia, S. P.; Bao, H.; Hines, M. A. *Surf. Sci.* **2003**, *541*, 252.
(75) Jakob, P.; Chabal, Y. J.; Kuhnke, K.; Christman, S. B. *Surf. Sci.* **1994**, *302*, 49.
(76) Kulkarni, M.; Green, S. K.; Shea, C.; Queeney, K. *J. Phys. Chem. C* **2009**, *113*, 10206.
(77) Pretsch, E.; Bühlmann, P.; Badertscher, M. *Structure Determination of Organic Compounds: Tables of Spectral Data*; Springer-Verlag: Berlin, 2009.
(78) Alecu, I. M.; Zheng, J.; Zhao, Y.; Truhlar, D. G. *J. Chem. Theory Comput.* **2010**, *6*, 2872.
(79) Jimenez-Hoyos, C. A.; Janesko, B. G.; Scuseria, G. E. *Phys. Chem. Chem. Phys.* **2008**, *10*, 6621.
(80) Chao, Y.; Siller, L.; Krishnamurthy, S.; Coxon, P. R.; Bangert, U.; Gass, M.; Kjeldgaard, L.; Patole, S. N.; Lie, L. H.; O'Farrell, N.; Alsop, T. A.; Houlton, A.; Horrocks, B. R. *Nat. Nanotechnol.* **2007**, *2*, 486.
(81) Wade, C. P.; Chidsey, C. E. D. *Appl. Phys. Lett.* **1997**, *71*, 1679.
(82) Perdew, J. P.; Burke, K.; Ernzerhof, M. *Phys. Rev. Lett.* **1996**, *77*, 3865.
(83) Kanai, Y.; Selloni, A. *J. Am. Chem. Soc.* **2006**, *128*, 3892.
(84) Takeuchi, N.; Kanai, Y.; Selloni, A. *J. Am. Chem. Soc.* **2004**, *126*, 15890.
(85) *CRC Handbook of Chemistry and Physics*, 95th ed.; Haynes, W. M., Ed.; CRC Press: Boca Raton, FL, 2014.
(86) Gross, T.; Oehme, H.; Kempe, R. *Organometallics* **1999**, *18*, 1815.

DOI: 10.1021/jacs.6b04962
J. Am. Chem. Soc. 2016, 138, 8639−8652